NUCL SCI TECH (2019) 30:62
https://doi.org/10.1007/s41365-019-0587-1

Simulation of the effects of different substrates, temperature, and substrate roughness on the mechanical properties of Al_2O_3 coating as tritium penetration barrier

Ze Liu[1] · Fei Meng[2] · Liang-Bi Yi[3]

Received: 5 July 2018 / Revised: 10 September 2018 / Accepted: 20 October 2018 / Published online: 14 March 2019

Abstract Residual thermal stress in the system is a serious problem that affects the application of tritium permeation barrier coatings in fusion reactors. The stress not only determines the adhesion between coating and substrate, but also changes the properties of the material. In this study, finite element analysis was used to investigate the relationship between the residual thermal stress and the mechanical properties of Al_2O_3 tritium penetration barrier systems. Moreover, the residual thermal stress influenced by factors such as different substrates, temperature, and substrate roughness was also analyzed. The calculation showed that the hardness and elastic modulus increased with increasing compressive stress. However, the hardness and elastic modulus decreased with increasing tensile stress. The systems composed of Al_2O_3 coatings and different substrates exhibited different trends in mechanical properties. As the temperature increased, the hardness and the elastic modulus increased in an Al_2O_3/316L stainless steel system; the trend was opposite in an Al_2O_3/Si system. Apart from this, the roughness of the substrate surface in the system could magnify the change in hardness and elastic modulus of the coating. Results showed that all these factors led to variation in the mechanical properties of Al_2O_3 tritium permeation barrier systems. Thus, the detailed reasons for the changes in mechanical properties of these materials need to be analyzed.

Keywords Finite element analysis · Thermal stress · Mechanical properties · Al_2O_3 tritium penetration barrier systems · Nanoindentation

✉ Ze Liu
liuze720@sina.com

1 Key Laboratory for Radiation Physics and Technology of Ministry of Education, Institute of Nuclear Science and Technology, Sichuan University, Chengdu 610064, China

2 Chengdu Youfang Technology Co., Ltd, Chengdu 610041, China

3 Southwestern Institute of Physics, Chengdu 610041, China

1 Introduction

To safely solve radioactive tritium problems and to optimize the balance of tritium in a fusion reactor, a tritium permeation barrier (TPB) deposited on the surface of structural materials can be used effectively to suppress tritium permeation. Many researchers have investigated different kinds of tritium permeation barriers such as nitrides (TiN, Si_3N_4, and Fe_2N) and oxides (Er_2O_3, Al_2O_3, Y_2O_3, and Cr_2O_3). The results show that these kinds of coatings are beneficial in minimizing tritium permeation. Among these materials, an Al_2O_3 coating is considered to be a promising candidate due to its good compatibility with liquid Pb–Li, excellent thermal stability, and high permeation reduction factor (PRF) [1–3].

Currently, several fabrication approaches [4, 5] such as plasma spraying (PS), chemical vapor deposition (CVD), and physical vapor deposition (PVD) are used to deposit an Al_2O_3 TPB coating. Among these methods, the PVD technique is a widely used method to prepare Al_2O_3 coatings [6]. During the PVD process, the residual stress that exists in the coating can limit the growth of the coating thickness and influence the microstructure and morphology of the coating [7]. The magnitude of residual stress can be affected by various factors such as substrate bias [8], gas precursor [9, 10], pressure [11, 12], and power density [13].

A great deal of effort has been made to determine the relationship between the residual stress and the mechanical properties of the material. Mani et al. [14] obtained the residual stress of a TiC coating by measuring the radius of curvature. They also analyzed the hardness of this coating by using a nanoindentation technique. The results showed that the compressive residual stress in the coating has a dominant relationship with its hardness rather than with the grain size. Bai et al. [15] studied the mechanical properties of CN_x coatings by nanoindentation experiments. They found that CN_x coatings with compressive residual stress have greater hardness and elastic modulus than those without compressive stress. Karlsson et al. [16] measured the residual stress in TiC_xN_{1-x} coatings using an X-ray diffraction method and obtained the elastic modulus of the coatings by nanoindentation. The results showed that the elastic modulus of the coating increases with the increase in negative stress in the coating. Chang et al. [17] studied a Ti coating that was deposited by radio frequency (RF) magnetron sputter and found that as the tensile stress increases, the elastic modulus of the coating decreases. Mallik et al. [18] investigated the mechanical properties of a Cu coating by a curvature method and found that the hardness in the coating gradually increases with increasing compressive stress. These studies showed that residual stress can affect the mechanical properties of the coating. However, the work focused on the residual stress in the coating and neglected the existence of the substrate, which can lead to the substrate effect [19, 20]. The substrate roughness, which affects the residual thermal stress distribution of the system, has also not been taken into consideration. Apart from this, few research studies explore the relationship between the residual thermal stress and the mechanical properties of the tritium permeation barrier.

In this study, the commercial software ANSYS, which is widely employed for solving engineering problems [21–23], was used to investigate the relationships between the mechanical properties of an Al_2O_3 tritium permeation barrier, residual thermal stress, temperature, and substrate roughness. We not only were concerned with the effect of residual thermal stress, but also paid attention to the substrate effect and its roughness. This process consisted of two steps. First, residual thermal stress was generated in the whole system by a change in temperature. Second, nanoindentation experiments were simulated by finite element analysis (FEA) to obtain the hardness and elastic modulus. Factors such as different substrates, temperature, and substrate roughness were then investigated.

2 Method

2.1 Theoretical background for nanoindentation

Nanoindentation is an efficient technique developed over the decades for measuring the hardness and the elastic modulus of thin coatings [24–27]. One of the advantages of this technique is that some of the mechanical properties can be obtained directly from a load–displacement curve. Another advantage is that the test can be performed on a very small scale. After the nanoindentation experiment, the imprint area can be found at the top surface of the specimen. The depth of the imprint is so extremely small that nanoindentation technology is considered to be nondestructive to the material. In addition, depth sensing technology, which replaces the measurement of the imprint area, is used in nanoindentation to measure the mechanical properties of the pressed material.

Fischer et al. [28] proposed a polynomial to describe the relationship between the projected area A_c and the contact depth h_c of the Berkovich indentation. The relationship between A_c and h_c can be shown as follows:

$$A_c \approx 24.5h_c^2. \tag{1}$$

The value of h_c can be measured by load–displacement data during nanoindentation experiments, and h_c is defined as

$$h_c = h_{max} - \varepsilon\frac{P_{max}}{S}, \tag{2}$$

where S is the contact stiffness, h_{max} is the maximum indentation depth, and ε is a geometry correction factor with a value of 0.75 for the Berkovich indenter. During the indenter unloading process, the relationship between the load P and the depth h can be determined as follows [29]:

$$P = A(h - h_f)^m, \tag{3}$$

where A is an indent constant, h_f is the final depth, and m depends on the geometry of the indenter. The elastic modulus of the sample can be derived from the initial unloading contact stiffness S, the formula for which is as follows [30]:

$$S = \mathrm{d}P/\mathrm{d}h(h_{max}) = mA(h_{max} - h_f)^{m-1}. \tag{4}$$

The relationship between the reduced elastic modulus (E_r), the contact stiffness (S), and the contact area (A_c) was obtained from Sneddon's work [31]; the formula is as follows:

$$E_r = \frac{1}{\beta}\frac{\sqrt{\pi}}{2}\frac{S}{\sqrt{A_c}}, \tag{5}$$

where the value of β depends on the geometry of the indenter and is 1.034 for the Berkovich indenter. The reduced elastic modulus E_r is expressed as follows:

$$\frac{1}{E_r} = \frac{1-v^2}{E} + \frac{1-v_i^2}{E_i}. \tag{6}$$

where v and E are the Poisson's ratio and elastic modulus of the specimen, and ν_i and E_i are the Poisson's ratio and elastic modulus of the indenter. King [32] provided a specific method for calculating the reduced elastic modulus E_r in a layered system:

$$\frac{1}{E_r} = \frac{1-v_i^2}{E_i} + \frac{1-v_f^2}{E_f}(1-\exp(-\alpha t/h_c)) + \frac{1-v_s^2}{E_s}(1 - \exp(-\alpha t/h_c)), \tag{7}$$

where t is the coating thickness. The subscripts s and f represent substrate and coating, respectively. α is a constant that equals 1.24 in this formula for the Berkovich indenter.

2.2 Analysis model

The residual thermal stress is generated from a heating or cooling process during deposition [33]. By using two steps in the FEA, we can investigate the relationship between residual thermal stress and the mechanical properties of an Al_2O_3 coating. The coating and substrate parameters, such as coefficient of thermal expansion (CTE), Poisson's ratio, and elastic modulus, affect the residual thermal stress significantly. The residual thermal stress formula is as follows [34]:

$$\sigma_{th} = \frac{E_c(\alpha_c - \alpha_s)}{1 - v_c}\Delta T, \tag{8}$$

where E_c is the elastic modulus of the coating, and α_c and α_s are the coefficients of thermal expansion of coating and substrate, respectively. v_c is the Poisson's ratio of the coating, and ΔT is the temperature difference.

Substrate materials consisting of 316L stainless steel (SS) and of silicon (Si) were used in the model to investigate the substrate effect. All calculations were performed by using two-dimension axisymmetric models. Furthermore, the roughness of substrate surface was described as a sinusoidal function [35]. The simplified axisymmetric coating/substrate model, which contained flat or rough substrates, is shown in Fig. 1. For the system with flat substrate, the coating thickness h was 2.2 μm and the substrate thickness H was 50 μm. For the rough substrate surface, the coating thickness h was defined as the distance from the top of the coating to the centerline of the wavy line. The coating and substrate thicknesses were same in both smooth and rough substrate systems. The amplitude A of the substrate surface was 1.2 μm, and the half wavelength L was 12.5 μm.

Lichinchi et al. [36] found that the sharpness of the Berkovich indenter has a great influence on the measurement of mechanical properties in a nanoindentation experiment. The ISO-14577 standard shows that the mean curvature radius of the Berkovich indenter ranges from 150 to 200 nm. Moreover, the elastic modulus and Poisson's ratio of the Berkovich indenter are 1140 GPa and 0.07, respectively. Thus, in the simulation, the indenter was considered as a rigid body containing a cone tip with a 150 nm rounding radius. A Berkovich indenter with a half-angle of 70.3° was used in this axisymmetric model. The indenter was driven into the model in a negative direction along the Y axis to a depth of 0.22 μm and at a speed of 44 nm/s. When the tip of the indenter reached the final position in the coating, the indenter began the unloading process. The large deflection option and Newton–Raphson method were used in the simulation.

Figure 2a shows the axisymmetric mesh and boundary condition. Due to the axial symmetry of the model, the PLAN182 elements in ANSYS were adopted for the calculation. To ensure the convergence of the calculation, a reasonable mesh was set for the whole system. Figure 2b shows that the most deformed region, which is under the indenter of the Al_2O_3 coating, had the finest mesh. The smallest elements measured 0.03 by 0.03 μm near the contact area between the coating and the indenter. Away from the center of contact, bias elements were set along the axis. A total of 12,474 quadrilateral elements and 38,044 nodes were meshed in the whole system. Fixed constraints were imposed on the left and bottom of the system where the nodes cannot move in the horizontal or vertical direction. All the other nodes could move according to the degrees of freedom.

Figure 3 shows the residual thermal stress distribution at different press-in positions (A, B, C) of the coating at 100 °C. The coating exhibits residual compressive stress, while most of the substrate region shows residual tensile stress. The residual compressive stress, located near the edge region, gradually increases. Compared to positions B and C, the residual thermal stress at the center point A in the coating is relatively uniform. Therefore, to avoid the impact of non-uniform stress on the indenter tip, point A was selected as the nanoindentation press-in position. In this manner, we could obtain the load–displacement curve by FEA. The properties of Al_2O_3, Si, and 316L SS were assumed to be isotropic and homogeneous, and the materials were modeled as having perfect elastic–plastic behavior. The mechanical properties of these materials at room temperature (RT = 23 °C) are shown in Table 1.

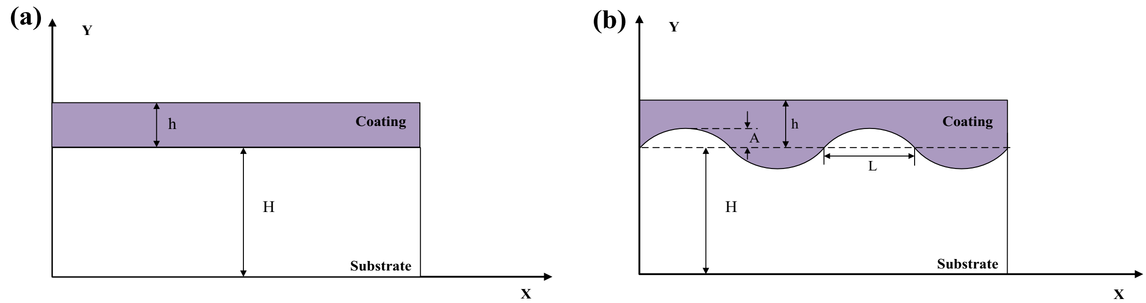

Fig. 1 The simplified schematic for axisymmetric Al_2O_3 coating systems with **a** flat substrate, **b** rough substrate

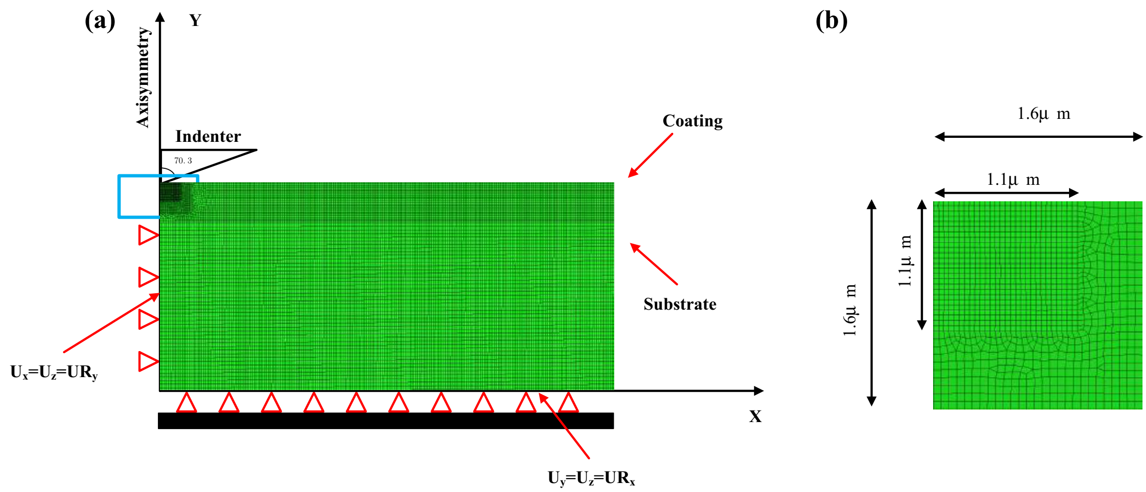

Fig. 2 (Color online) The axisymmetric mesh used in the nanoindenter simulation: **a** mesh overview and boundary condition for the overall system, **b** the detail of mesh in the region of contact beneath the Berkovich indenter tip

Fig. 3 (Color online) Nanoindentation position along the *X* axis

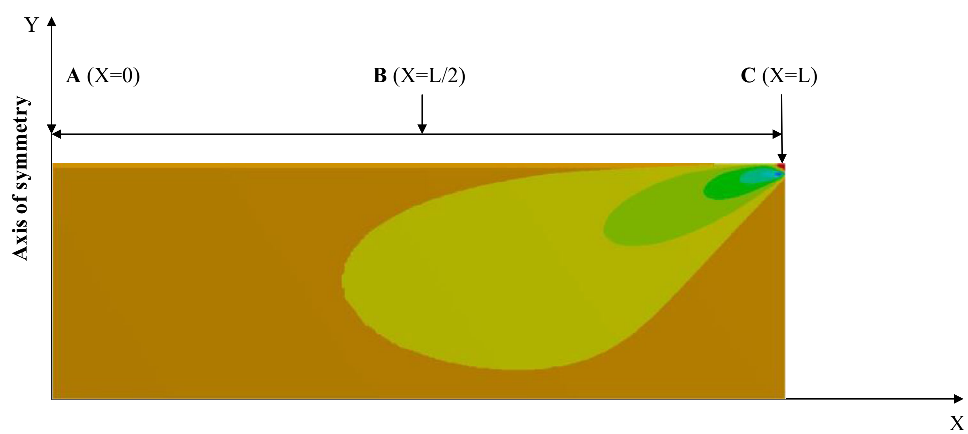

Table 1 Material properties at room temperature (23 °C) [37–41]

Properties	Materials		
	Al_2O_3	316L SS	Si
Poisson's ratio	0.22	0.28	0.224
Elastic modulus (GPa)	375	198	164.4
Coefficient of thermal expansion ($10^{-6}\times$ °C^{-1})	8.4	14.7	3.2
Yield strength (MPa)	15,400	195	4410

3 Results and discussion

3.1 Effect of residual thermal stress on different substrates

Figure 4 shows the distribution of stress at ± 100 °C for the Al_2O_3/316L SS and Al_2O_3/Si systems. When the temperature of the Al_2O_3/316L SS system rises to 100 °C ($\Delta T > 0$) from room temperature (RT), the Al_2O_3 coating shows a negative shear stress. When the temperature drops from RT to − 100 °C ($\Delta T < 0$), the Al_2O_3 coating shows a positive shear stress. Comparison of the Al_2O_3/316L SS system to the Al_2O_3/Si system at the same temperature shows that the shear stress distribution of the Al_2O_3/316L SS system is significantly opposite to that of Al_2O_3/Si system, as illustrated in Fig. 3c and d. The reason is that the CTE of the Al_2O_3 coating is larger than that of the Si

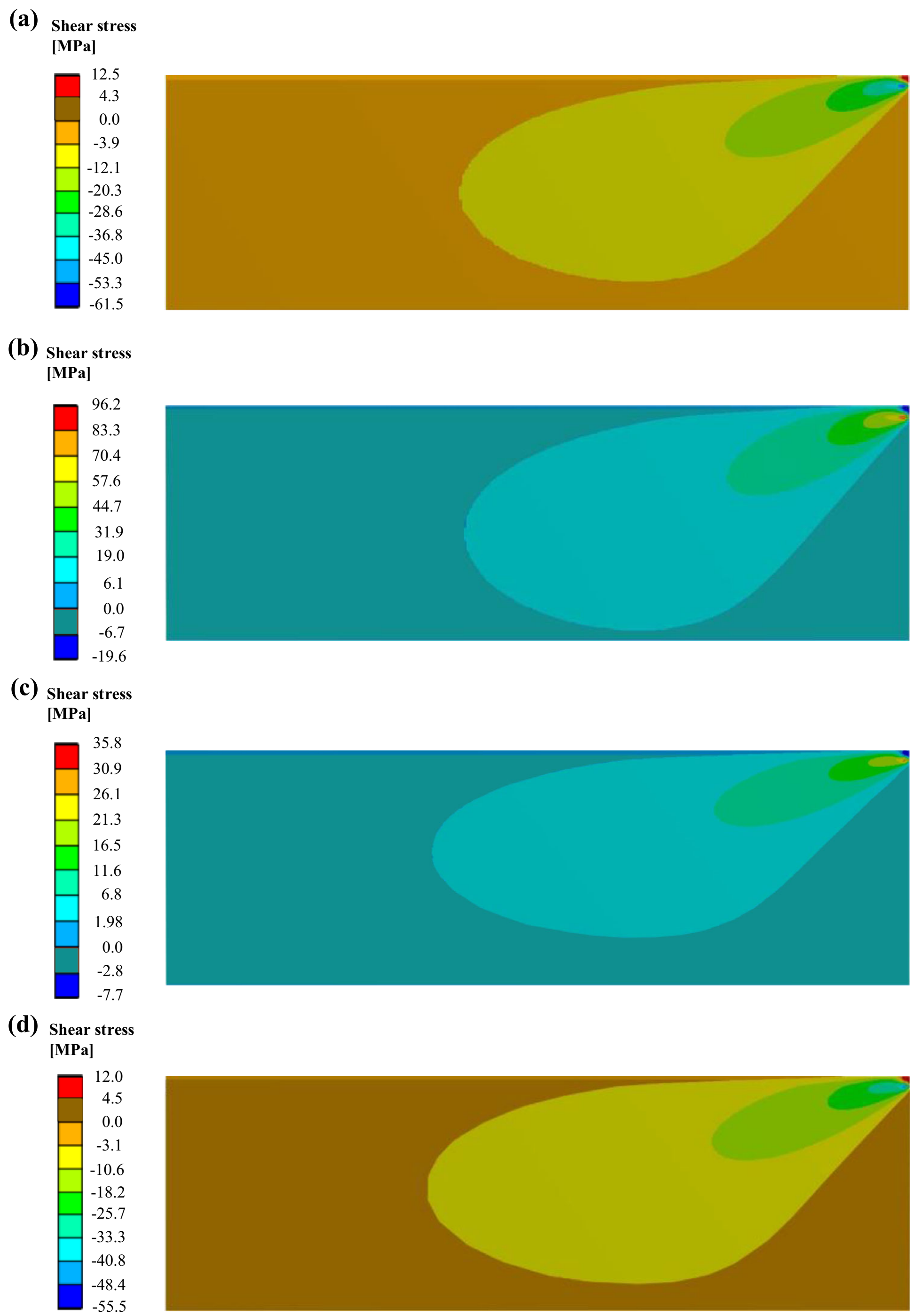

Fig. 4 (Color online) Distribution of stress for **a** Al_2O_3/316L SS system at + 100 °C, **b** Al_2O_3/316L SS system at − 100 °C, **c** Al_2O_3/Si system at + 100 °C, **d** Al_2O_3/Si system at − 100 °C

substrate but smaller than that of the 316L SS substrate, as shown in Eq. 8.

For simplicity, only the simulation process of nanoindentation at RT is shown in Fig. 5. When the equivalent stress reaches the yield strength of the material, plastic deformation begins to occur. The formula for calculating the equivalent stress is as follows:

$$\sigma = \sqrt{\frac{(\sigma_1 - \sigma_2)^2 + (\sigma_2 - \sigma_3)^2 + (\sigma_1 - \sigma_3)^2}{2}}, \quad (9)$$

where σ_1, σ_2, and σ_3 represent the first, second, and third principal stresses generated at each point in the sample. As shown in Fig. 5b, the equivalent stress is nearly 75.61 GPa when the indenter is at the final depth of the loading process. Furthermore, the value of stress is greater than the yield strength of Al_2O_3 (see Table 1), which indicates that the stress beneath the tip of the indenter reached the yield limit of the Al_2O_3 coating before the indenter stopped at the lowest position. As the indenter unloading progresses, the zone of elastic deformation in the coating gradually decreases to zero and plastic deformation results in an indentation footprint, as shown in Fig. 5c.

Figures 6 and 7 show the effect of residual thermal stress on hardness and elastic modulus of the Al_2O_3/316L SS system and Al_2O_3/Si system. In both these systems, the changes in the residual thermal stress in the coatings are

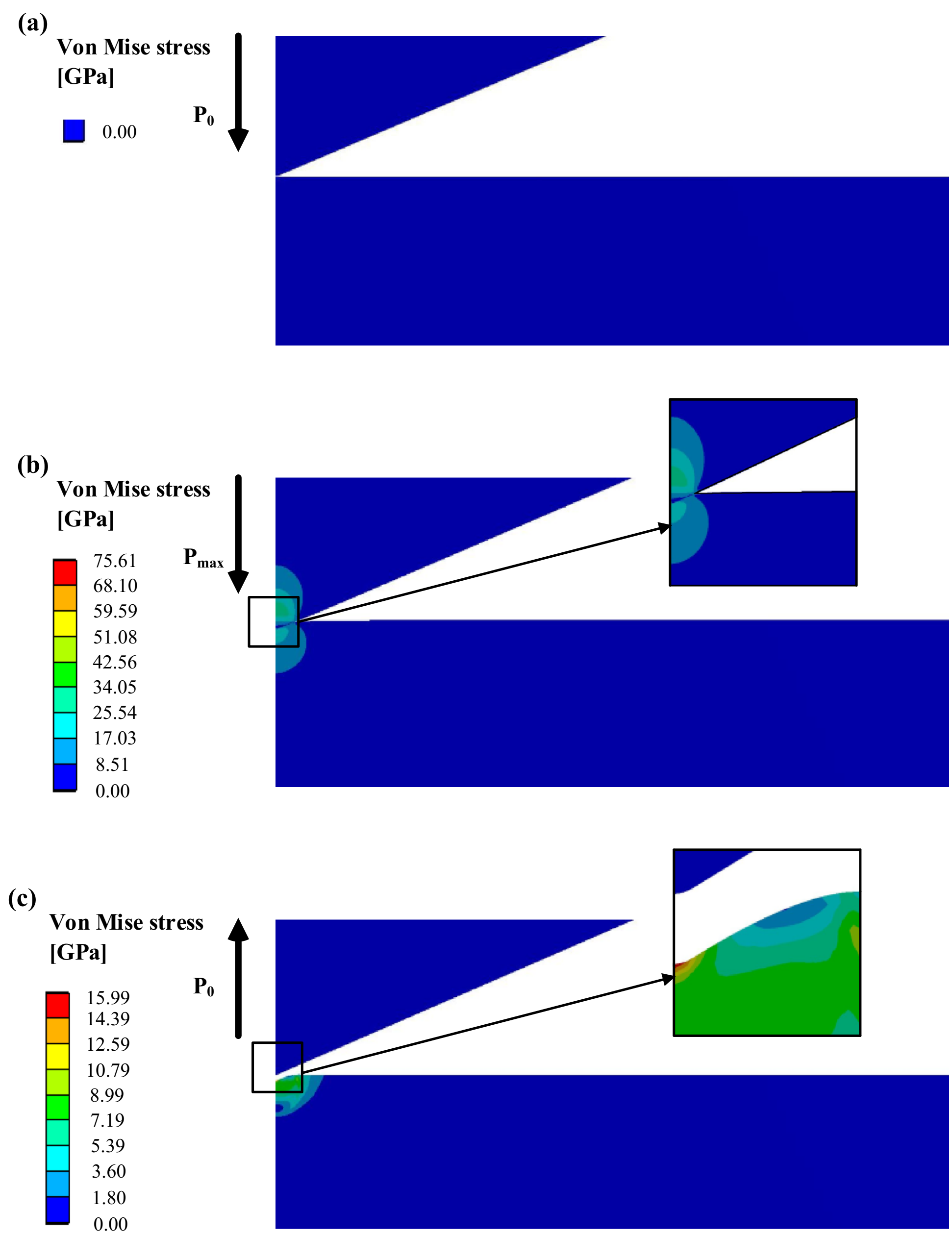

Fig. 5 (Color online) Stress distribution of the Al_2O_3/316L SS system **a** before loading of indenter, **b** after loading of indenter, and **c** after unloading of indenter

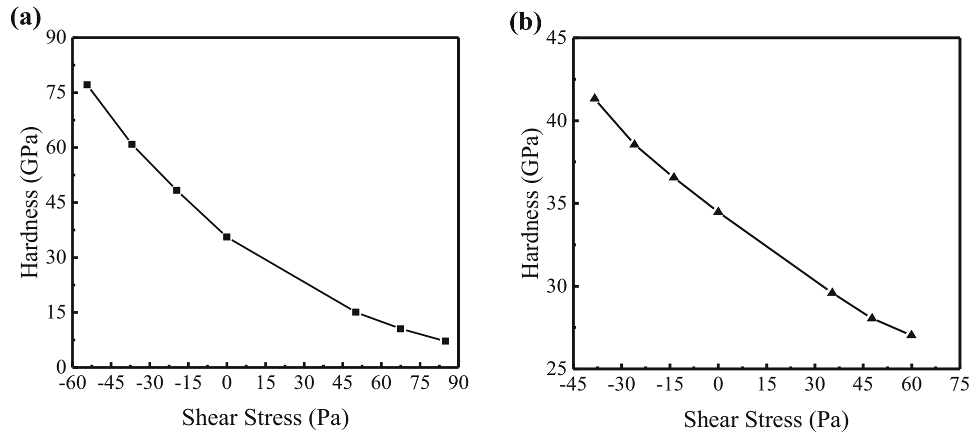

Fig. 6 Effect of residual thermal stress on hardness of **a** Al_2O_3/316L stainless steel system, **b** Al_2O_3/Si system

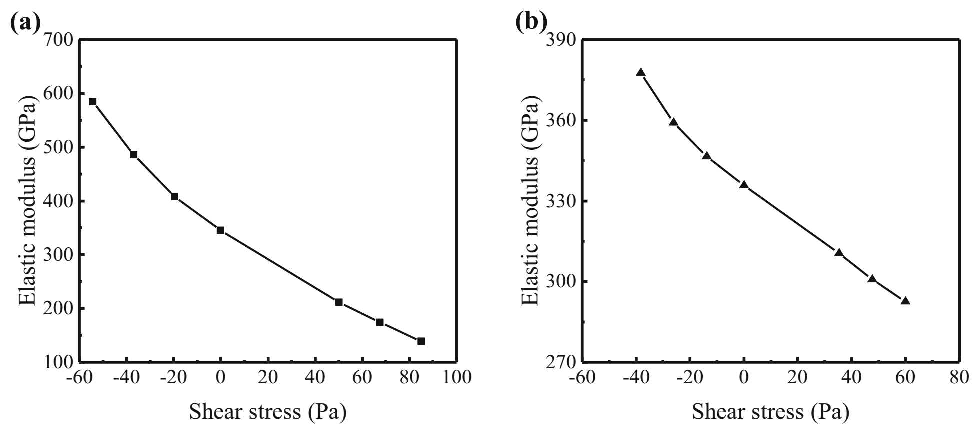

Fig. 7 Effect of residual thermal stress on elastic modulus of **a** Al_2O_3/316L stainless steel system, **b** Al_2O_3/Si system

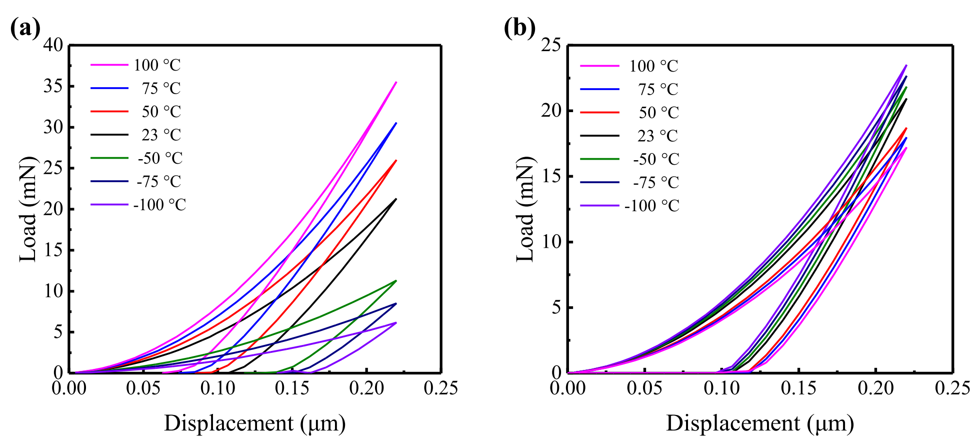

Fig. 8 (Color online) Simulated load–displacement curves at different temperature for **a** Al_2O_3/316L stainless steel system, **b** Al_2O_3/Si system

inversely proportional to their hardness and elastic modulus. For positive shear stress, hardness and elastic modulus decrease with increasing shear stress. The trend is reversed for negative shear stress. These results indicate that the compressive shear stress can improve both the hardness and elastic modulus of the coating. However, the tensile shear stress can reduce the hardness and elastic modulus of the coating. These analysis results are similar to results obtained previously by the present authors [15, 16, 42].

Shear stress can determine the adhesion between the coating and the substrate [43]. For example, compressive shear stress can help to increase the adhesive strength and tensile stress can prompt initiation and propagation of cracks. The properties of the substrate material determine the distribution of residual thermal stress in the coating, which influences to varying degrees the coating's mechanical properties. From the aspect of residual thermal stress, this is another "substrate effect". As shown in

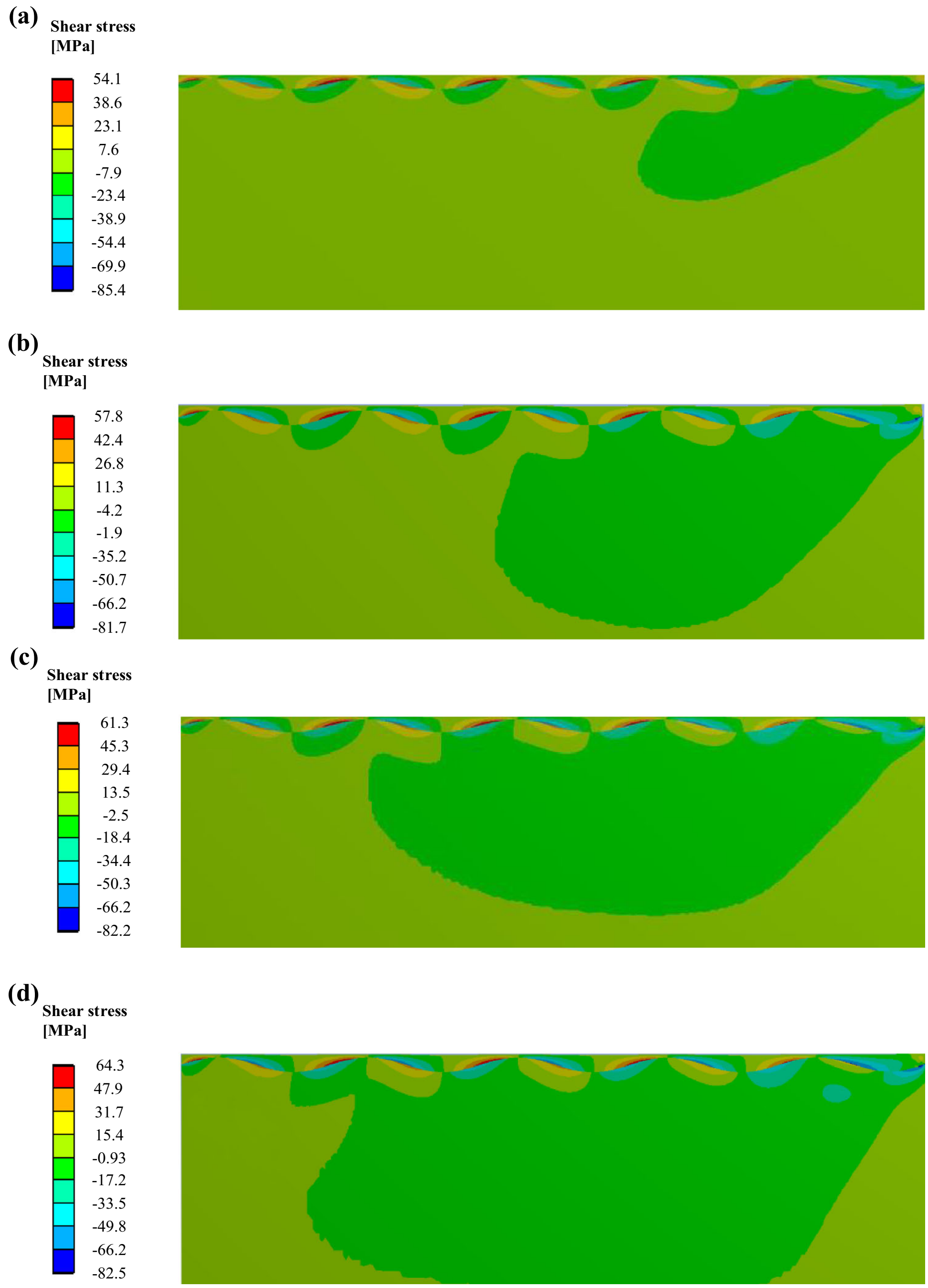

Fig. 9 (Color online) Shear stress distribution in the Al_2O_3/316L SS systems with different amplitudes of substrates **a** A = 1.2 μm, **b** A = 1.3 μm, **c** A = 1.4 μm, and **d** A = 1.5 μm

Figs. 6 and 7, for the 316L SS substrate system, when the coating is subjected to compressive stress, the slopes of hardness and elastic modulus are approximately -1.2×10^9 and -5.07×10^9, respectively. When the coating is subjected to tensile stress, the slopes of hardness and elastic modulus are approximately -0.23×10^9 and -2.08×10^9, respectively. For the Si substrate system, when the coating is subjected to compressive stress, the slopes of hardness and elastic modulus are approximately -0.9×10^9 and -1.27×10^9, respectively. When the coating is subjected to tensile stress, the slopes of hardness and elastic modulus are approximately -0.1×10^8 and -7.3×10^8, respectively. These data show that, for the same substrate material, the effect of residual thermal stress on the elastic modulus is greater than that on the hardness of the coating. Furthermore, the substrate material determines the varying degrees of hardness and elastic modulus of the coating.

Figure 8 shows the load–displacement curves for the systems with 316L SS and with Si substrates at different temperatures. For the Al_2O_3/316L SS system, the load–displacement curve shifts to the left as the system

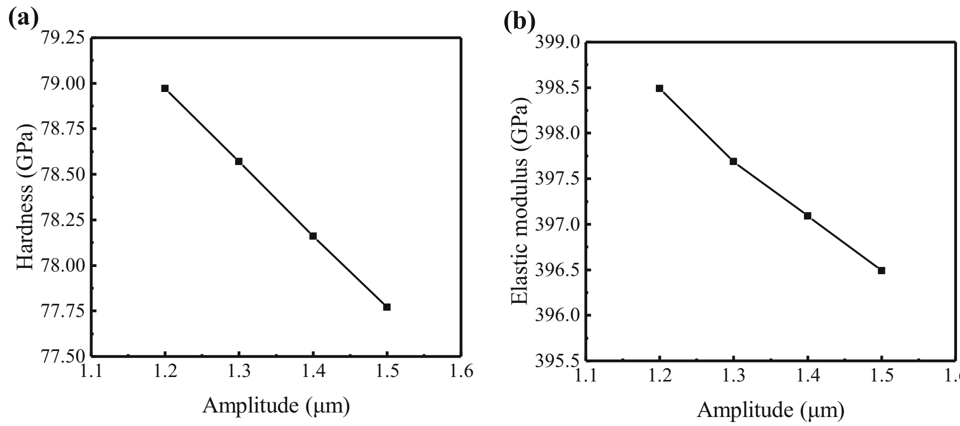

Fig. 10 Effect of amplitude of substrate surface on **a** hardness and **b** elastic modulus in Al_2O_3/316L SS system

temperature increases. The trend for the Al_2O_3/Si system is opposite. The reason is that the temperature determines the magnitude of the residual thermal stress, which is determined by the CTE between coating and substrate. As the temperature increases, the residual compressive stress in the coating gradually increases in the Al_2O_3/316L SS system. Meanwhile, the residual tensile stress in the coating increases in the Al_2O_3/Si system as the temperature increases. The residual thermal stress further influences the degree of curve drift. The trends of the load–displacement curves imply that when the coating is subjected to compressive stress in either Al_2O_3/316L SS system or Al_2O_3/Si system, the curve shifts to the left (to smaller displacements) and vice versa. Similar observations have been reported by Wei and Yang [20].

The load stress of the Berkovich indenter increases with the increase in temperature to achieve the same displacement, as shown in Fig. 8a. This result further indicates that the hardness of coating increases with the increase in temperature. The trend is opposite for the Al_2O_3/Si system as shown in Fig. 8b. Sarikaya [44] investigated the effect of temperature on an Al_2O_3 coating deposited on a stainless steel substrate. He found that as the temperature increased from 25 to 500 °C in the coating/substrate system, the hardness of the coating increased. Thus, the trend obtained in the present study is consistent with the work by Sarikaya.

3.2 Relationship between substrate roughness and mechanical properties

The effect of residual thermal stress on hardness and elastic modulus is magnified by introducing roughness of the substrate. For simplicity, only the Al_2O_3/316L SS systems with different amplitudes at 100 °C are shown here. Figure 9 shows the effect of increasing substrate amplitude on residual thermal stress in the systems. In contrast to the Al_2O_3/316L SS system with smooth substrate, the existence of surface amplitude results in an increase in residual thermal stress. Furthermore, the residual thermal stress increases with increasing amplitude of the substrate. The region with a positive slope of the sinusoidal curve acts as a stress concentrator. The compressive stress in the edge region of the substrate gradually expands as substrate amplitude increases. Figure 10 demonstrates that the hardness and elastic modulus decrease with the increase in amplitude of the substrate. Furthermore, the amplitude of the substrate surface shows an approximately linear relationship with hardness and elastic modulus. The trend of Al_2O_3 coating hardness change, obtained by FEA, is similar to that in the previous work [44].

4 Conclusion

To study the effect of factors such as different substrates, temperature, and substrate roughness on mechanical properties of Al_2O_3 tritium permeation barrier systems, axisymmetric finite element models were used to simulate the distribution of residual thermal stress and the process of nanoindentation. The main results demonstrate the following:

1. The substrates of different materials, such as 316L SS and Si, influence the mechanical properties of the Al_2O_3 coating. As the temperature changes, the substrate determines the rate of variability of the coating's hardness and elastic modulus. Furthermore, for the same substrate material, the effect of residual thermal stress on the elastic modulus is greater than that on the hardness of the coating.
2. When the coating is subjected to compressive stress, the hardness and elastic modulus increase. However, when the coating is subjected to tensile stress, the hardness and elastic modulus decrease. The load–displacement curve of nanoindentation shifts to the left

as the compressive stress in the coating increases. The curve shifts to the right as the tensile stress in the coating increases.

3. Compared to a smooth substrate, a substrate with rough surface causes stress concentration, which magnifies changes in the hardness and elastic modulus of the coating.

References

1. D. Levchuk, F. Koch, H. Maier et al., Deuterium permeation through Eurofer and α-alumina coated Eurofer. J. Nucl. Mater. **328**, 103–106 (2004). https://doi.org/10.1016/j.jnucmat.2004.03.008
2. A. Aiello, A. Ciampichetti, G. Benamati, An overview on tritium permeation barrier development for WCLL blanket concept. J. Nucl. Mater. **329**, 1398–1402 (2004). https://doi.org/10.1016/j.jnucmat.2004.04.205
3. T. Wang, J. Pu, C. Bo et al., Sol–gel prepared Al_2O_3 coatings for the application as tritium permeation barrier. Fusion Eng. Des. **85**, 1068–1072 (2010). https://doi.org/10.1016/j.fusengdes.2010.01.021
4. G. Benamati, C. Chabrol, A. Perujo, E. Rigal, H. Glasbrenner, Development of tritium permeation barriers on Al base in Europe. J. Nucl. Mater. **271**, 391–395 (1999). https://doi.org/10.1016/S0022-3115(98)00792-2
5. X. Xiang, X. Wang, G.K. Guo et al., Preparation technique and alloying effect of aluminide coatings as tritium permeation barriers: a review. J. Hydrog. Energy **40**, 3697–3707 (2015). https://doi.org/10.1016/j.ijhydene.2015.01.052
6. T. Lee, W.K. Kim, Y.J. Lee et al., Effect of Al_2O_3 coatings prepared by RF sputtering on polyethylene separators for high-power lithium ion batteries. Macromol. Res. **22**, 1190–1195 (2014). https://doi.org/10.1007/s13233-014-2163-1
7. S. Kumar, D. Sarangi, P.N. Dixit et al., Diamond-like carbon films with extremely low stress. Thin Solid Films **346**, 130–137 (1999). https://doi.org/10.1016/S0040-6090(98)01500-4
8. M. Ban, T. Hasegawa, S. Fujii et al., Stress and structural properties of diamond-like carbon films deposited by electron beam excited plasma CVD. Diam. Relat. Mater. **12**, 47–56 (2003). https://doi.org/10.1016/S0925-9635(02)00265-0
9. Y. Oka, M. Kirinuki, Y. Nishimura et al., Measurement of residual stress in DLC films prepared by plasma-based ion implantation and deposition. Surf. Coat. Technol. **186**, 141–145 (2004). https://doi.org/10.1016/j.surfcoat.2004.04.010
10. V. Teixeira, Mechanical integrity in PVD coatings due to the presence of residual stresses. Thin Solid Films **392**, 276–281 (2001). https://doi.org/10.1016/S0040-6090(01)01043-4
11. S. Zhang, H. Xie, X. Zeng et al., Residual stress characterization of diamond-like carbon coatings by an X-ray diffraction method. Surf. Coat. Technol. **122**, 219–224 (1999). https://doi.org/10.1016/S0257-8972(99)00298-4
12. M.M. Morshed, B.P. McNamara, D.C. Cameron et al., Stress and adhesion in DLC coatings on 316L stainless steel deposited by a neutral beam source. J. Mater. Process. Technol. **141**, 127–131 (2003). https://doi.org/10.1016/S0924-0136(03)00246-2
13. M.M. Morshed, D.C. Cameron, B.P. McNamara et al., DLC films deposited by a neutral beam source: adhesion to biological implant metals. Surf. Coat. Technol. **169**, 254–257 (2003). https://doi.org/10.1016/S0257-8972(03)00179-8
14. A. Mani, P. Aubert, F. Mercier et al., Effects of residual stress on the mechanical and structural properties of TiC thin films grown by RF sputtering. Surf. Coat. Technol. **194**, 190–195 (2005). https://doi.org/10.1016/j.surfcoat.2004.06.017
15. M. Bai, K. Kato, N. Umehara et al., Nanoindentation and FEM study of the effect of internal stress on micro/nano mechanical property of thin CN_x films. Thin Solid Films **377**, 138–147 (2000). https://doi.org/10.1016/S0040-6090(00)01314-6
16. L. Karlsson, L. Hultman, J.E. Sundgren, Influence of residual stresses on the mechanical properties of TiC_xN_{1-x} (x = 0, 0.15, 0.45) thin films deposited by arc evaporation. Thin Solid Films **371**, 167–177 (2000). https://doi.org/10.1016/s0040-6090(00)00996-2
17. R.C. Chang, F.Y. Chen, C.T. Chuang et al., Residual stresses of sputtering titanium thin films at various substrate temperatures. Nanosci. Nanotechnol. **10**, 4562–4567 (2010). https://doi.org/10.1166/jnn.2010.1696
18. A. Mallik, B.C. Ray, Residual stress and nanomechanical properties of sonoelectrodeposited Cu films. Surf. Eng. **27**, 551–556 (2011). https://doi.org/10.1179/1743294411Y.0000000011
19. O. Borrero-López, M. Hoffman, A. Bendavid et al., Substrate effects on the mechanical properties and contact damage of diamond-like carbon thin films. Diam. Relat. Mater. **19**, 1273–1280 (2010). https://doi.org/10.1016/j.diamond.2010.06.004
20. C. Wei, J.Y. Yen, Effect of film thickness and interlayer on the adhesion strength of diamond like carbon films on different substrates. Diam. Relat. Mater. **16**, 1325–1330 (2007). https://doi.org/10.1016/j.diamond.2007.02.003
21. D. Zhu, J. Chen, Thermal stress analysis on chemical vapor deposition tungsten coating as plasma facing material for EAST. J. Nucl. Mater. **455**, 185–188 (2014). https://doi.org/10.1016/j.jnucmat.2014.05.054
22. L.M. Jin, N.X. Wang, W.Q. Zhu et al., FEA-based structural optimization design of a side cooling collimating mirror at SSRF. Nucl. Sci. Tech. **28**, 159 (2017). https://doi.org/10.1007/s41365-017-0307-7
23. J.B. Yu, J.X. Chen, L. Kang et al., Thermal analysis and tests of W/Cu brazing for primary collimator scraper in CSNS/RCS. Nucl. Sci. Tech. **28**, 46 (2017). https://doi.org/10.1007/s41365-017-0208-9
24. A. Karimzadeh, M.R. Ayatollahi, M. Alizadeh, Finite element simulation of nano-indentation experiment on aluminum 1100. Comp. Mater. Sci. **81**, 595–600 (2014). https://doi.org/10.1016/j.commatsci.2013.09.019
25. L. Gan, B. Ben-Nissan, The effects of mechanical properties of thin films on nano-indentation data: finite element analysis. Comp. Mater. Sci. **8**, 273–281 (1997). https://doi.org/10.1016/s0927-0256(97)97-2
26. X. Chen, J. Yan, A.M. Karlsson, On the determination of residual stress and mechanical properties by indentation. Mater. Sci. Eng., A **416**, 139–149 (2006). https://doi.org/10.1016/j.msea.2005.10.034
27. M. Kot, W. Rakowski, J.M. Lackner et al., Analysis of spherical indentations of coating-substrate systems: experiments and finite element modeling. Mater. Des. **43**, 99–111 (2013). https://doi.org/10.1016/j.matdes.2012.06.040
28. A.C. Fischer-Cripps, *Nanoindentation Instrumentation* (Springer, New York, 2011)
29. W.C. Oliver, G.M. Pharr, An improved technique for determining hardness and elastic modulus using load and displacement sensing indentation experiments. J. Mater. Res. **7**, 1564–1583 (1992). https://doi.org/10.1557/JMR.1992.1564
30. M.F. Doerner, D.S. Gardner, W.D. Nix, Plastic properties of thin films on substrates as measured by submicron indentation hardness and substrate curvature techniques. J. Mater. Res. **1**, 845–851 (1986). https://doi.org/10.1557/JMR.1986.0845

31. I.N. Sneddon, The relation between load and penetration in the axisymmetric Boussinesq problem for a punch of arbitrary profile. Int. J. Eng. Sci. **3**, 47–57 (1965). https://doi.org/10.1016/0020-7225(65)90019-4
32. R.B. King, Elastic analysis of some punch problems for a layered medium. Int. J. Solids Struct. **23**, 1657–1664 (1987). https://doi.org/10.1016/0020-7683(87)90116-8
33. R. Elsing, O. Knotek, U. Balting, Calculation of residual thermal stress in plasma-sprayed coatings. Surf. Coat. Technol. **43**, 416–425 (1990). https://doi.org/10.1016/0257-8972(90)90093-R
34. C. Wei, J.F. Yang, A finite element analysis of the effects of residual stress, substrate roughness and non-uniform stress distribution on the mechanical properties of diamond-like carbon films. Diam. Relat. Mater. **20**, 839–844 (2011). https://doi.org/10.1016/j.diamond.2011.04.004
35. W.X. Zhang, X.L. Fan, T.J. Wang, The surface cracking behavior in air plasma sprayed thermal barrier coating system incorporating interface roughness effect. Appl. Surf. Sci. **258**, 811–817 (2011). https://doi.org/10.1016/j.apsusc.2011.08.103
36. M. Lichinchi, C. Lenardi, J. Haupt et al., Simulation of Berkovich nanoindentation experiments on thin films using finite element method. Thin Solid Films **312**, 240–248 (1998). https://doi.org/10.1016/S0040-609000739-6(97)
37. Y. Wu, S. Zhu, T. Liu et al., The adhesion strength and deuterium permeation property of SiC films synthesized by magnetron sputtering. Appl. Surf. Sci. **307**, 615–620 (2014). https://doi.org/10.1016/j.ijhydene.2016.04.233
38. H. Liu, J. Tao, Y. Gautreau et al., Simulation of thermal stresses in SiC–Al_2O_3 composite tritium penetration barrier by finite-element analysis. Mater. Des. **30**, 2785–2790 (2009). https://doi.org/10.1016/j.matdes.2009.01.025
39. M. Grujicic, H. Zhao, Optimization of 316 stainless steel/alumina functionally graded material for reduction of damage induced by thermal residual stresses. Mater. Sci. Eng. A **252**, 117–132 (1998). https://doi.org/10.1016/s0921-5093(98)98-2
40. H. Pelletier, J. Krier, A. Cornet et al., Limits of using bilinear stress–strain curve for finite element modeling of nanoindentation response on bulk materials. Thin Solid Films **379**, 147–155 (2000). https://doi.org/10.1016/s0040-6090(00)01559-5
41. Z. Liu, G.G. Yu, A.P. He et al., Simulation of thermal stress in Er_2O_3 and Al_2O_3 tritium penetration barriers by finite-element analysis. Plasma Sci. Technol **19**, 095602 (2017). https://doi.org/10.1088/2058-6272/aa719d
42. G. Cheng, D. Han, C. Liang, Influence of residual stress on mechanical properties of TiAlN thin films. Surf. Coat. Tech. **228**, 328–330 (2013). https://doi.org/10.1016/j.surfcoat.2012.05.108
43. D.J. Ward, A.F. Williams, Finite element simulation of the development of residual stress in IAPVD films. Thin Solid Films **355**, 311–315 (1999). https://doi.org/10.1016/S0040-6090(99)00507
44. O. Sarikaya, Effect of some parameters on microstructure and hardness of alumina coatings prepared by the air plasma spraying process. Surf. Coat. Tech. **190**, 388–393 (2005). https://doi.org/10.1016/j.surfcoat.2004.02.007